**Supporting Information**

# A high phase transition temperature organic–inorganic Sn(IV)-based metal halide designed by applying amino positional isomerism to the cation

Zhang-Tian Xia‡, Hui-Ping Chen‡, Jun-Chao Qi, Hang Peng, Xin Shen, Yong-Ju Bai, Zhen-Yu Wang, Tian-En Yang, Wei-Qiang Liao*

*Ordered Matter Science Research Center, Nanchang University, Nanchang 330031, People's Republic of China*

* Corresponding author. E-mail: liaowq@ncu.edu.cn

‡ These authors contributed equally to this work.

∗ Corresponding author.

*E-mail address: liaowq@ncu.edu.cn (W. Liao).*

**Experiment Section**

**Sample preparation**. *n*-Butylamine, *sec*-butylamine, $SnCl_4$ and hydrochloric acid are commercially available and do not require further purification. To the mixed solution of *n*-butylamine (10 mmol, 0.73 g) and 10 mL of hydrochloric acid, $SnCl_4$ (5 mmol, 1.30 g) was added. The mixture was stirred until a clear solution was obtained. After slow evaporation for one week at 323 K, colorless $[NBA]_2SnCl_6$ crystals were collected with a yield of 90%. Following a similar synthesis procedure as for $[NBA]_2SnCl_6$, $SnCl_4$ (5 mmol, 1.30 g) was added to the mixed solution of *sec*-butylamine (10 mmol, 0.73 g) and 10 mL of hydrochloric acid. The mixture was stirred until the solution was completely clear. After slow evaporation for one week at 323 K, colorless $[SBA]_2SnCl_6$ crystals were collected with a yield of 85%.

**Single crystal X-ray diffraction and PXRD measurement.** The single-crystal diffraction data of $[NBA]_2SnCl_6$ and $[SBA]_2SnCl_6$ were collected on Rigaku Oxford Diffraction XtaLAB Synergy X-ray diffractometer with *Cu*-Kα radiation (λ = 1.54184 Å). We used the Crystal Clear software package to process the data. The crystal structures were solved by using the *SHELXLTL* software package. All the non-hydrogen atoms were refined anisotropically and the H atoms were placed at their geometrically calculated positions. PXRD measurement was performed on a Rigaku SmartLab X-ray diffractometer, with a step size of 0.02°.

**Measurement methods.** The IR spectra of $[NBA]_2SnCl_6$ and $[SBA]_2SnCl_6$ in KBr pellets were recorded on a Shimadzu IR Prestige-21 instrument at room temperature and DSC experiments were carried out on PerkinElmer DSC 6000. The measurements were performed at a heating and cooling rate of 20 K $min^{-1}$ under the protection of $N_2$. TGA measurement was performed on the PerkinElmer TGA 8000 in the temperature range of 300 K to 1000 K with a heating rate of 30 K $min^{-1}$ under $N_2$ atmosphere. The real part ($\varepsilon'$) of complex permittivity was measured on a Tonghui TH2828A impedance analyzer under the frequency of 1 MHz. The measuring AC voltage was 1 V. Silver conduction paste deposited on pressed powder pellet surfaces was used as the electrodes. Ultraviolet-visible (UV-vis) absorption spectrum data was obtained by using Shimadzu (Tokyo, Japan) UV-3600 Plus spectrophotometer with an ISR-2600 Plus integrating sphere operating from 200 nm to 800 nm at room temperature.

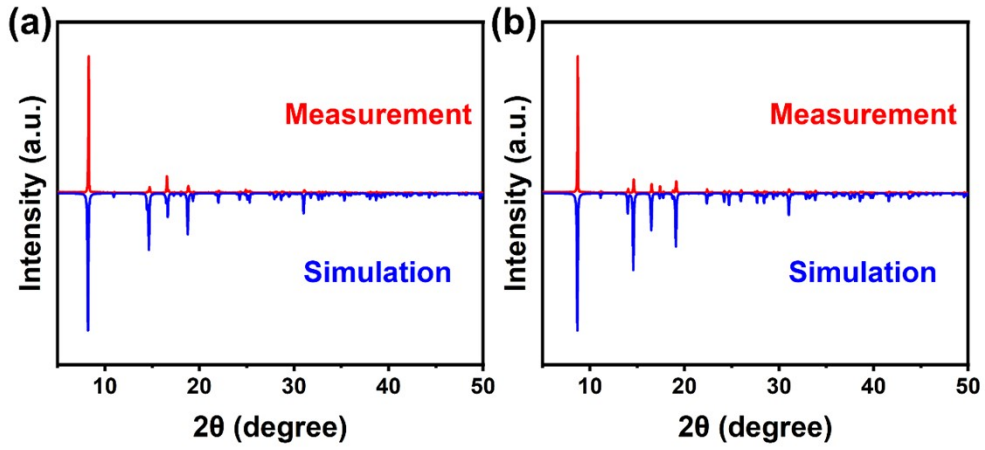


**Fig. S1.** PXRD measurement and simulation patterns of $[NBA]_2SnCl_6$ (a) and $[SBA]_2SnCl_6$ (b) at 298 K.

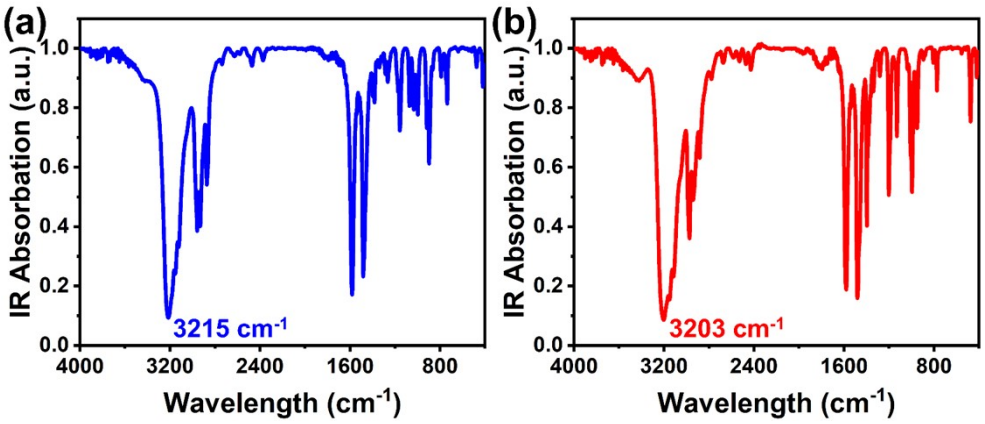


**Fig. S2.** IR spectra of $[NBA]_2SnCl_6$ (a) and $[SBA]_2SnCl_6$ (b).

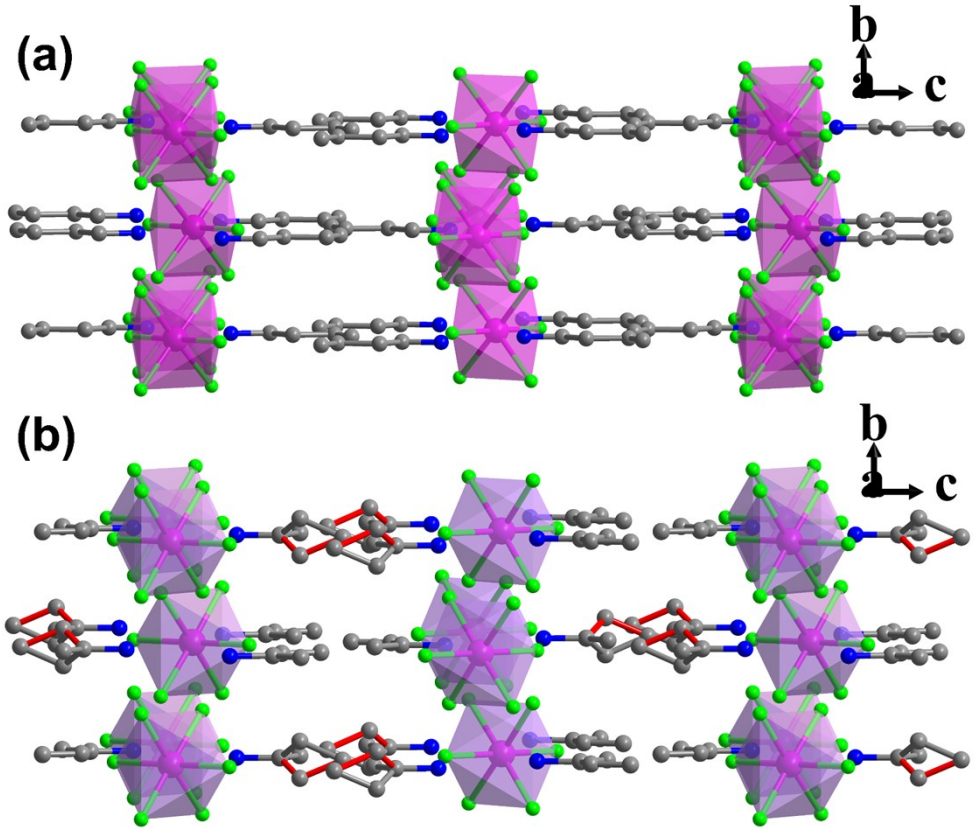


**Fig. S3.** Packing view of the crystal structure of $[NBA]_2SnCl_6$ (a) and $[SBA]_2SnCl_6$ (b) at 298 K along the *a*-axis. Hydrogen atoms are omitted for clarity. The chemical bonds highlighted in red represent the disordered part.

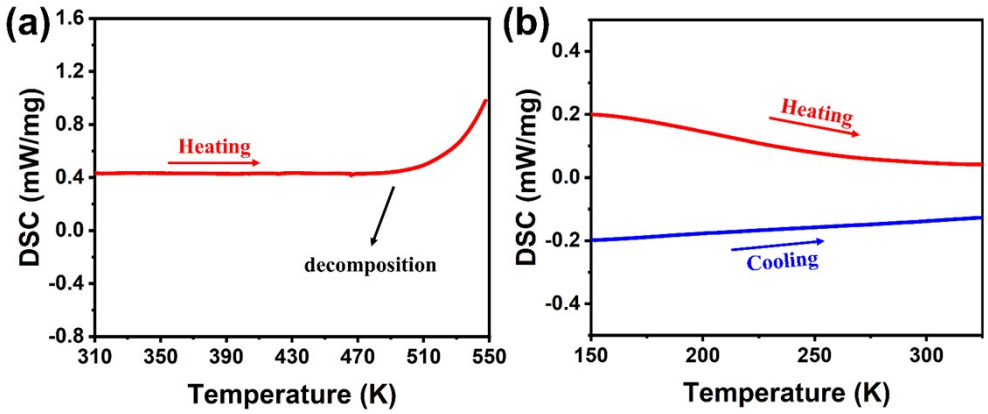


**Fig. S4.** DSC curves of $[NBA]_2SnCl_6$ (a) and $[SBA]_2SnCl_6$ (b).

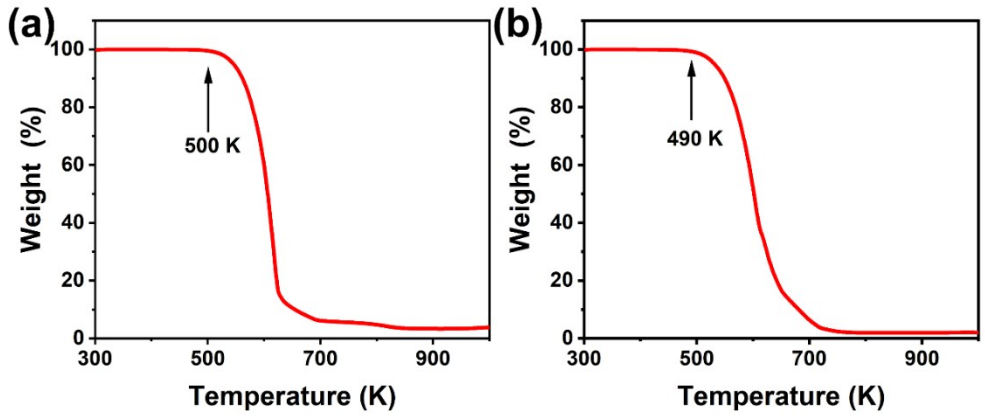


**Fig. S5.** The TGA curves of $[NBA]_2SnCl_6$ (a) and $[SBA]_2SnCl_6$ (b).

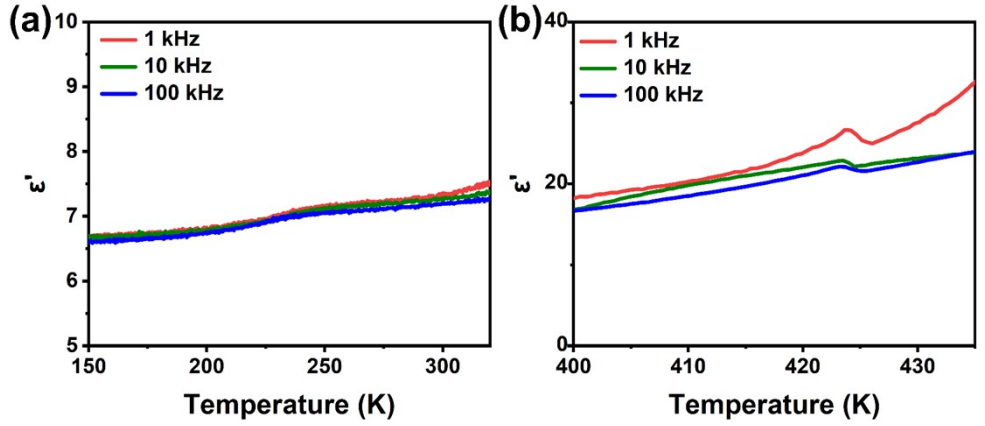


**Fig. S6.** Temperature dependence of the dielectric real part ($\varepsilon'$) of $[NBA]_2SnCl_6$ (a) and $[SBA]_2SnCl_6$ (b) at 1 kHz, 10 kHz, 100 kHz upon cooling.

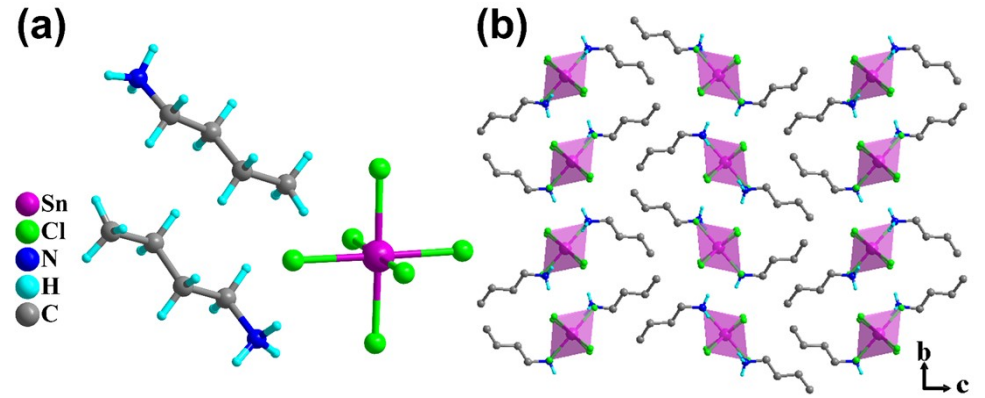


**Fig. S7.** Basic unit (a) and packing view (b) of the crystal structure of $[NBA]_2SnCl_6$ at 173 K. Some hydrogen atoms are omitted for clarity.

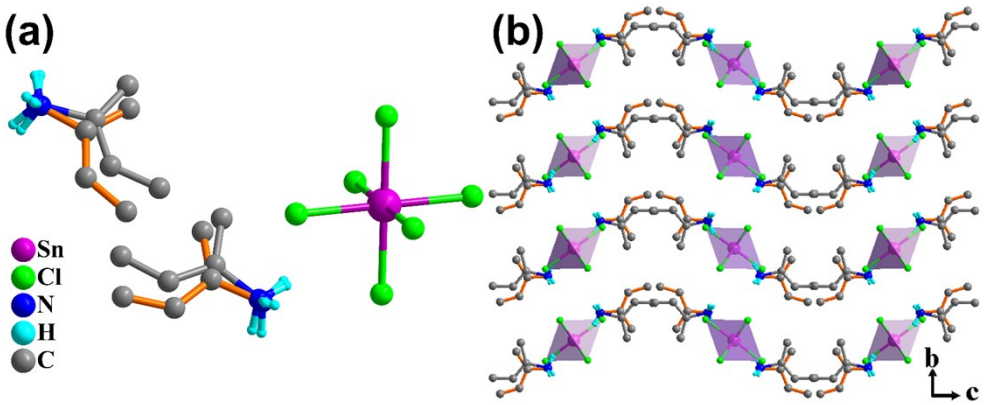


**Fig. S8.** Basic unit (a) and packing view (b) of the crystal structure of $[SBA]_2SnCl_6$ at 443 K. Some hydrogen atoms are omitted for clarity. The chemical bonds highlighted in orange represent the disordered part.

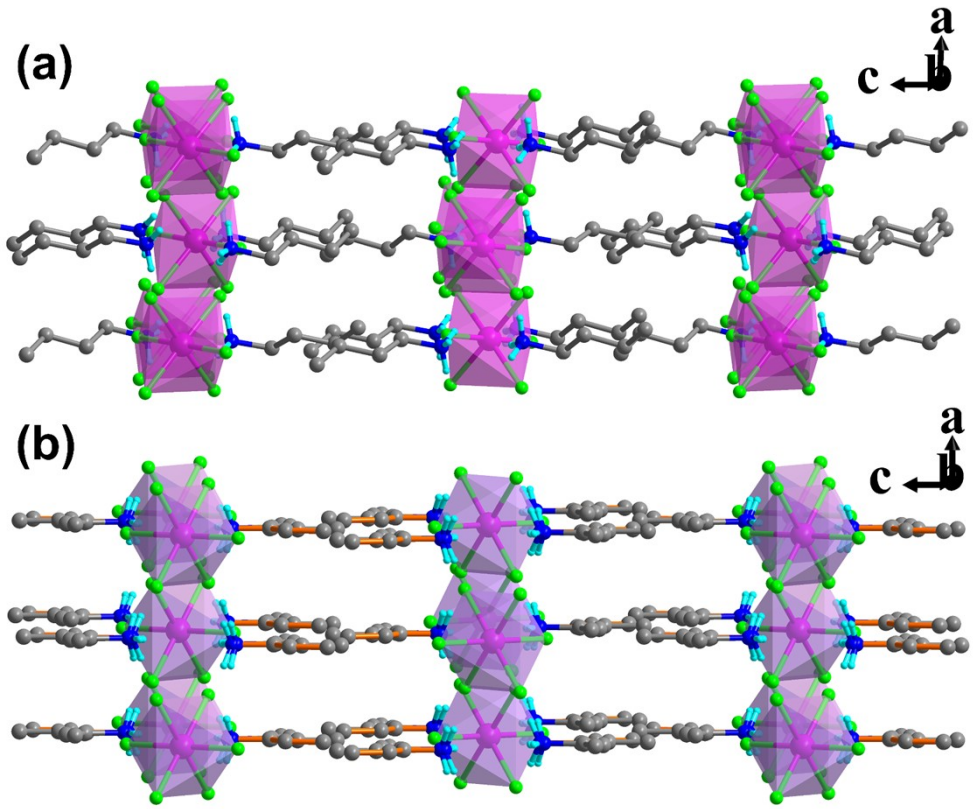


**Fig. S9.** Packing view of the crystal structure of $[NBA]_2SnCl_6$ (a) at 173 K and $[SBA]_2SnCl_6$ (b) at 443 K along the *b*-axis. Some hydrogen atoms are omitted for clarity. The chemical bonds highlighted in orange represent the disordered part.

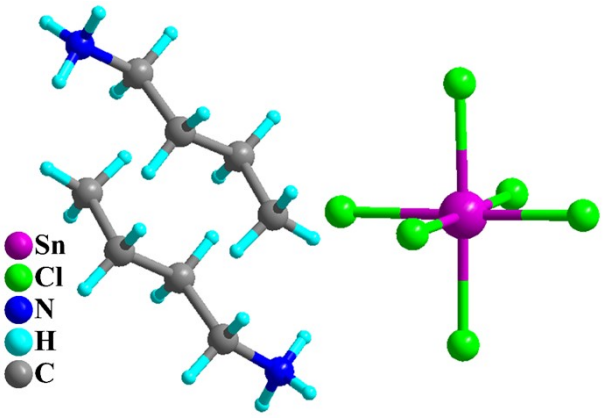


**Fig. S10.** Basic unit of $[NBA]_2SnCl_6$ at 443 K. Some hydrogen atoms are omitted for clarity.

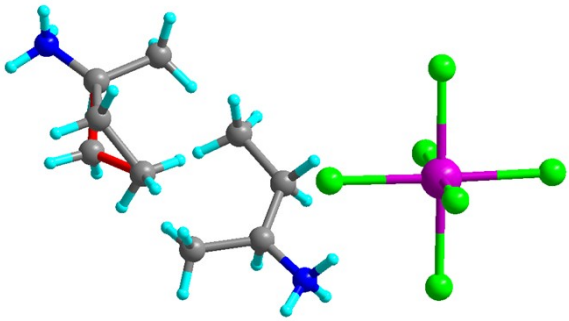

**Fig. S11.** Basic unit of $[SBA]_2SnCl_6$ at 173 K. Some hydrogen atoms are omitted for clarity. The chemical bonds highlighted in red represent the disordered part.

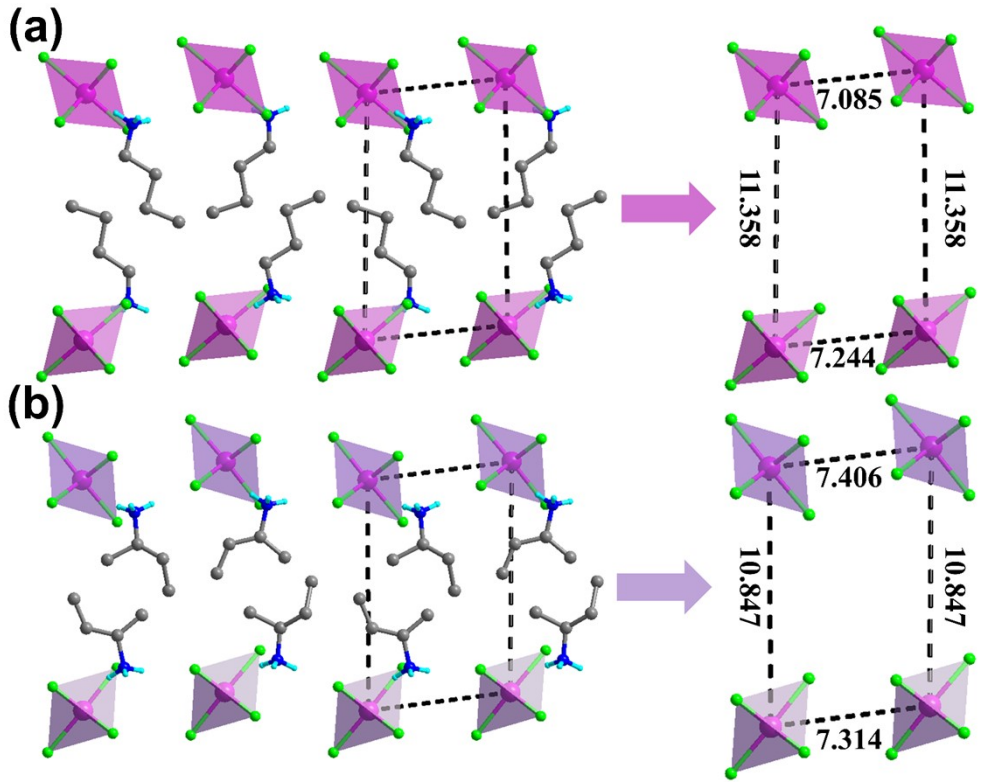


**Fig. S12.** The quadrilateral void formed by four nearest-neighbor Sn atoms in $[NBA]_2SnCl_6$ (a) and $[SBA]_2SnCl_6$ (b) at 298 K. The numbers (Å) indicate the distances between adjacent Sn atoms. Some hydrogen atoms are omitted for clarity.

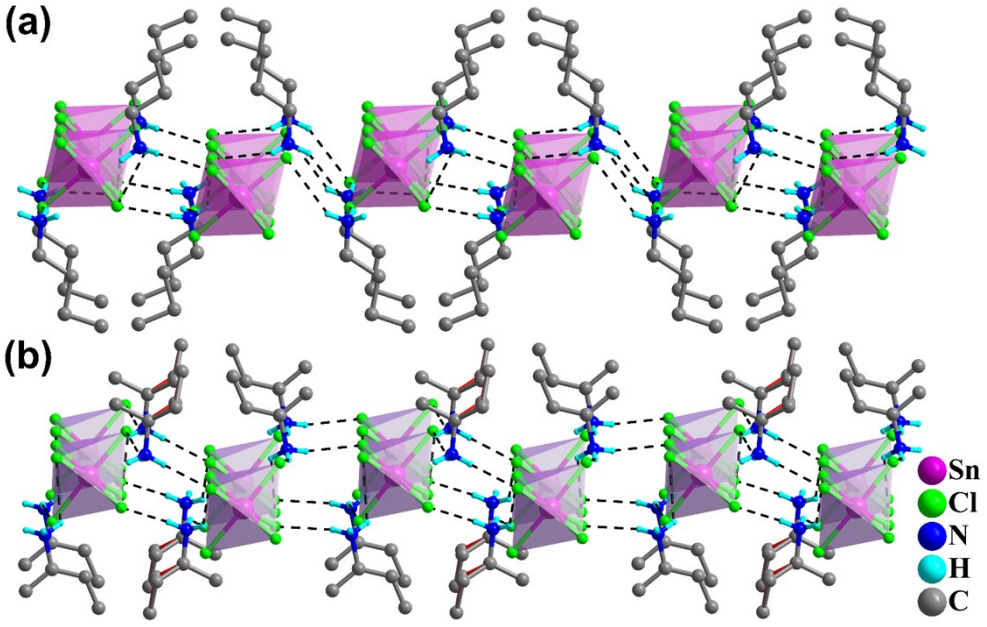


**Fig. S13.** Hydrogen bond interaction between anions and cations of $[NBA]_2SnCl_6$ (a) and $[SBA]_2SnCl_6$ (b) at 298 K. Some hydrogen atoms are omitted for clarity. The chemical bonds highlighted in red represent the disordered part.

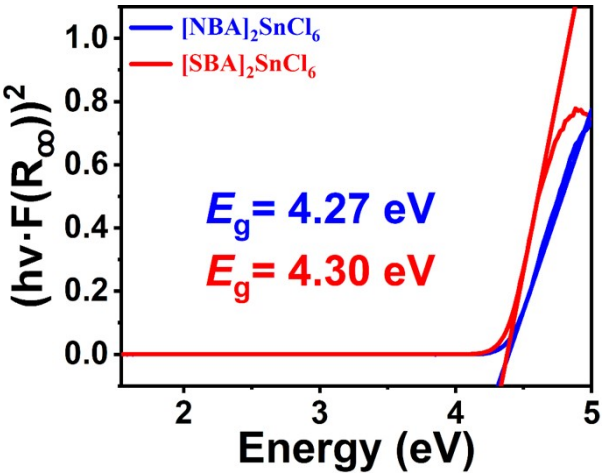


**Fig. S14.** Plot of $(hv \cdot F(R_\infty))^2$ *vs*. $hv$ for determination of direct band gap of $[NBA]_2SnCl_6$ and $[SBA]_2SnCl_6$.

**Table S1.** The crystal data and structure refinements of $[NBA]_2SnCl_6$ and $[SBA]_2SnCl_6$ at 173 K, 298 K and 443 K.

| | **$[NBA]_2SnCl_6$** | | | **$[SBA]_2SnCl_6$** | | |
|---|---|---|---|---|---|---|
| Temperature | 173 K | 298 K | 443 K | 173 K | 298 K | 443 K |
| Weight | 479.68 | 479.68 | 479.68 | 479.68 | 479.68 | 479.68 |
| Crystal system | Monoclinic | Orthorhombic | Orthorhombic | Orthorhombic | Orthorhombic | Orthorhombic |
| Space group | $P2_1/n$ | *Pnma* | *Pnma* | *Pnma* | *Pnma* | *Cmca* |
| *a*/Å | 7.1876(2) | 12.2341(2) | 12.3988(6) | 12.5723(2) | 12.6465(3) | 7.4642(9) |
| *b*/Å | 12.1044(3) | 7.3350(1) | 7.4445(4) | 7.25440(10) | 7.3518(1) | 12.5882(16) |
| *c*/Å | 21.6094(5) | 21.4976(4) | 21.6749(13) | 20.2943(3) | 20.4097(5) | 21.926(4) |
| $\alpha$/° | 90 | 90 | 90 | 90 | 90 | 90 |
| $\beta$/° | 92.298(2) | 90 | 90 | 90 | 90 | 90 |
| $\gamma$/° | 90 | 90 | 90 | 90 | 90 | 90 |
| Volume/Å$^3$ | 1878.54(8) | 1929.13(5) | 2000.66(19) | 1850.93(5) | 1897.58(7) | 2060.2(5) |
| *Z* | 4 | 4 | 4 | 4 | 4 | 4 |
| $R_1$ [$I>2\sigma(I)$] | 0.0506 | 0.0718 | 0.0568 | 0.0452 | 0.0470 | 0.0738 |
| $wR_2$ [$I>2\sigma(I)$] | 0.1733 | 0.2061 | 0.1662 | 0.1222 | 0.1309 | 0.2377 |
| GOF | 1.091 | 1.090 | 1.075 | 1.065 | 1.087 | 1.072 |

**Table S2.** The $T_c$ of some typical OIMH phase transition materials.

| **Compounds** | **$T_c$** | **References** |
|---|---|---|
| $(C_8H_{10}ClN)_2SnCl_6$ | 377 K | 1 |
| (*S*-3-OH-piperidinium)$_2SnCl_6$ | 401 K | 2 |
| $[Br(CH_2)_3NH_3]_2SnCl_6$ | 284.24 K | 3 |
| $[Br(CH_2)_3NH_3]_2SnBr_6$ | 301.89 K | 3 |
| $[(CH_2)_4NHCH_3]_2SnBr_6$ | 352 K | 4 |
| $[CH_3PH_3]SnI_3$ | 298 K | 5 |
| $[2\text{-}(H_3NCH_2)(C_5H_4NH)]SbI_5$ | 360 K and 390 K | 6 |
| (piperidinium)$_2SbCl_5$ | 338 K | 7 |
| $[NH_3CH_2CH_2F]_3BiCl_6$ | 361.5 K | 8 |
| $[CH_3CH_2NH_3]_2BiBr_5$ | 120 K and 160 K | 9 |
| $CH_3NH_3PbI_3$ | 330 K | 10 |
| (4,4-difluorocyclohexylammonium)$_2PbI_4$ | 377 K | 11 |
| [*R*(*S*)-N-(1-phenylethyl)ethane-1,2-diaminium]$_2PbI_4$ | 389 K | 12 |
| (3-fluorobenzyltrimethylammonium)$PbBr_3$ | 420 K | 13 |
| $(C_5NH_{13}Br)_2PbBr_4$ | 392 K | 14 |
| (Trimethyliodomethylammonium)$PbCl_3$ | 345 K and 358 K | 15 |
| $[CH_3CH_2NH_3]_4Pb_3Cl_{10}$ | 415 K | 16 |
| $[ICH_2N(CH_3)_3]PbI_3$ | 312 K | 17 |
| $[I(CH_2)_3NH_2CH_3]_2PbI_4$ | 390 K | 18 |
| $[((CH_2)_2CF_2(CH_2)_2)NH_2]_2PbI_4$ | 428.5 K | 19 |
| (N-fluoroethyl-N-methylmorpholine)$PbBr_3$ | 343 K | 20 |

| | | |
|---|---|---|
| (4,4-difluorocyclohexylammonium)$_2$PbBr$_4$ | 409 K | 21 |
| [4,4-difluoropiperidinium]$_2$PbI$_4$ | 428.5 K | 22 |
| (2-fluorobenzylammonium)$_2$PbCl$_4$ | 448 K | 23 |
| [SBA]$_2$SnCl$_6$ | 430 K | this work |

**Table S3.** Selected bond lengths/Å and bond angles/° for compound [NBA]$_2$SnCl$_6$ at 298 K.

| | Bond lengths | | Bond angles | |
|---|---|---|---|---|
| **298 K** | Sn1—Cl1 | 2.416(1) | Cl1—Sn1—Cl1$^{I}$ | 92.39(8) |
| | Sn1—Cl1$^{I}$ | 2.416(1) | Cl1—Sn1—Cl2 | 88.81(5) |
| | Sn1—Cl2 | 2.423(2) | Cl1—Sn1—Cl3$^{I}$ | 88.55(6) |
| | Sn1—Cl3 | 2.428(1) | Cl1—Sn1—Cl4 | 91.32(6) |
| | Sn1—Cl3$^{I}$ | 2.428(1) | Cl1$^{I}$—Sn1—Cl2 | 88.81(5) |
| | Sn1—Cl4 | 2.407(2) | Cl1$^{I}$—Sn1—Cl3 | 88.55(6) |
| | | | Cl1$^{I}$—Sn1—Cl4 | 91.32(6) |
| | | | Cl2—Sn1—Cl3 | 90.17(6) |
| | | | Cl2—Sn1—Cl3$^{I}$ | 90.17(6) |
| | | | Cl3—Sn1—Cl3$^{I}$ | 90.49(7) |
| | | | Cl3—Sn1—Cl4 | 89.70(5) |
| | | | Cl3$^{I}$—Sn1—Cl4 | 89.70(5) |

Symmetry code(s): (I) [+x, -1/2-y, +z]

**Table S4.** The selected hydrogen bond lengths [Å] and bond angles [°] of [NBA]$_2$SnCl$_6$ at 298 K.

| D—H···A | D—H /Å | H···A /Å | D···A /Å | D—H···A /° |
|---|---|---|---|---|
| N1-H1A···Cl2$^{I}$ | 0.890 | 2.771 | 3.538 | 145.11 |
| N1-H1B…Cl1$^{II}$ | 0.890 | 2.874 | 3.549 | 133.87 |
| N1-H1C…Cl1 | 0.890 | 2.930 | 3.549 | 128.20 |
| N1-H2A…Cl3$^{III}$ | 0.890 | 2.839 | 3.377 | 120.30 |
| N2-H2B…Cl3$^{IV}$ | 0.890 | 2.552 | 3.430 | 169.14 |
| N2-H2C…Cl3$^{V}$ | 0.890 | 2.727 | 3.377 | 130.80 |

Symmetry code(s): (I) [-x, -1/2+y, 1-z], (II) [+x, -3/2-y, +z], (III) [+x, -1+y, +z], (IV) [1-x, -1/2+y, 1-z], (V) [+x, -1/2-y, +z]

**Table S5.** Selected bond lengths/Å and bond angles/° for compound $[SBA]_2SnCl_6$ at 298 K.

| | Bond lengths | | Bond angles | |
|---|---|---|---|---|
| **298 K** | Sn1—Cl1 | 2.405(1) | Cl1—Sn1—$Cl1^I$ | 92.05(7) |
| | Sn1—$Cl1^I$ | 2.405(1) | Cl1—Sn1—Cl2 | 89.59(4) |
| | Sn1—Cl2 | 2.428(2) | Cl1—Sn1—$Cl3^I$ | 89.37(5) |
| | Sn1—Cl3 | 2.427(1) | Cl1—Sn1—Cl4 | 91.81(5) |
| | Sn1—$Cl3^I$ | 2.427(1) | $Cl1^I$—Sn1—Cl2 | 89.59(4) |
| | Sn1—Cl4 | 2.428(1) | $Cl1^I$—Sn1—Cl3 | 89.37(5) |
| | | | $Cl1^I$—Sn1—Cl4 | 91.81(5) |
| | | | Cl2—Sn1—Cl3 | 89.95(5) |
| | | | Cl2—Sn1—$Cl3^I$ | 89.95(5) |
| | | | Cl3—Sn1—$Cl3^I$ | 89.19(8) |
| | | | Cl3—Sn1—Cl4 | 88.62(5) |
| | | | $Cl3^I$—Sn1—Cl4 | 88.62(5) |

Symmetry code(s): (I) [+x, 3/2-y, +z]

**Table S6.** The selected hydrogen bond lengths [Å] and bond angles [°] of $[SBA]_2SnCl_6$ at 298 K.

| D—H···A | D—H /Å | H···A /Å | D···A /Å | D—H···A /° |
|---|---|---|---|---|
| N1-H1A···$Cl1^I$ | 0.890 | 2.926 | 3.533 | 126.98 |
| N1-H1B…Cl1 | 0.890 | 2.910 | 3.533 | 152.03 |
| N1-H1C…$Cl1^{II}$ | 0.890 | 2.710 | 3.587 | 128.47 |
| N1-H2A…$Cl3^{III}$ | 0.890 | 2.614 | 3.322 | 137.17 |
| N2-H2B…$Cl3^{IV}$ | 0.890 | 2.541 | 3.405 | 163.90 |
| N2-H2C…$Cl3^V$ | 0.890 | 2.681 | 3.322 | 129.75 |

Symmetry code(s): (I) [+x, 5/2-y, +z], (II) [2-x, -1/2+y, 1-z], (III) [+x, 7/2-y, +z], (IV) [1-x, -1/2+y, 1-z], (V) [+x, -1+y, +z]

**Table S7.** Selected bond lengths/Å and bond angles/° for compound $[NBA]_2SnCl_6$ at 173 K.

| | Bond lengths | | Bond angles | |
|---|---|---|---|---|
| **173 K** | Sn1—Cl1 | 2.434(2) | Cl1—Sn1—Cl2 | 88.95(6) |
| | Sn1—Cl2 | 2.420 (2) | Cl1—Sn1—Cl4 | 90.43(6) |
| | Sn1—Cl3 | 2.422(2) | Cl1—Sn1—Cl5 | 89.77(6) |
| | Sn1—Cl4 | 2.429(2) | Cl1—Sn1—Cl6 | 90.20(6) |
| | Sn1—Cl5 | 2.418(2) | Cl2—Sn1—Cl3 | 91.87(6) |
| | Sn1—Cl6 | 2.433(2) | Cl2—Sn1—Cl5 | 90.88(6) |
| | | | Cl2—Sn1—Cl6 | 88.72(6) |
| | | | Cl3—Sn1—Cl4 | 88.74(6) |
| | | | Cl3—Sn1—Cl5 | 90.79(6) |
| | | | Cl3—Sn1—Cl6 | 89.24(6) |
| | | | Cl4—Sn1—Cl5 | 90.20(6) |
| | | | Cl4—Sn1—Cl6 | 90.20(6) |

**Table S8.** Selected bond lengths/Å and bond angles/° for compound $[SBA]_2SnCl_6$ at 443 K.

| | Bond lengths | | Bond angles | |
|---|---|---|---|---|
| **443 K** | Sn1—Cl1 | 2.408(3) | Cl1—Sn1—Cl2 | 91.23(1) |
| | Sn1—$Cl1^{I}$ | 2.408(3) | Cl1—Sn1—$Cl2^{I}$ | 88.77(2) |
| | Sn1—$Cl1^{II}$ | 2.408(3) | Cl1—Sn1—$Cl1^{I}$ | 92.39(2) |
| | Sn1—$Cl1^{III}$ | 2.408(3) | Cl1—Sn1—$Cl1^{II}$ | 92.39(2) |
| | Sn1—Cl2 | 2.411(4) | $Cl1^{I}$—Sn1—Cl2 | 88.77(2) |
| | Sn1—$Cl2^{I}$ | 2.411(4) | $Cl1^{I}$—Sn1—$Cl2^{I}$ | 91.23(1) |
| | | | $Cl1^{I}$—Sn1—$Cl1^{II}$ | 87.61(2) |
| | | | $Cl1^{I}$—Sn1—$Cl1^{III}$ | 92.39(2) |
| | | | $Cl1^{II}$—Sn1—Cl2 | 91.23(1) |
| | | | $Cl1^{II}$—Sn1—$Cl2^{I}$ | 88.77(1) |
| | | | $Cl1^{III}$—Sn1—Cl2 | 87.61(2) |
| | | | $Cl1^{III}$—Sn1—$Cl2^{I}$ | 91.23(1) |

Symmetry code(s): (I) [-x, 1-y, -z]; (II) [-x, +y, +z]; (III) [+x, 1-y, 1-z]

**References:**


1. M. N. Wang, Y. X. Luo, M. Zhao, M. Zhao, F. X. Wang, X. W. Fan and Y. H. Tan, A Lead-Free Tin Organic-Inorganic Hybrid Material with Reversible Phase Transition and Fluorescent Properties. *ChemSelect.*, 2024, **9**, e202401502.

2. M.L. Ren, Wang Luo, Z. J. Xu, H. K. Li, L. Liu, C. Shi, N. Wang, H. Y. Ye and L. P. Miao, H/OH substitution achieving high-temperature multiferroicity in a Sn(IV)-based hybrid perovskite, *Inorg. Chem. Front.*, 2024, **11**, 7617-7622.
3. G. Teri, H.F. Ni, Q.F. Luo, X.P. Wang, J.Q. Wang, D.W. Fu and Q. Guo, Tin-based organic–inorganic metal halides with a reversible phase transition and thermochromic response, *Mater. Chem. Front.*, 2023, **7**, 2235-2240.
4. X.X. Hu, H.J. Xu, W.Q. Guo, S.G. Han, Y. Liu, Y. Ma, Q.S. Fan, J.H. Luo and Z.H Sun, $[C_5H_{12}N]_2SnBr_6$: a lead-free phase transition compound with switchable quadratic nonlinear optical properties, *Mater. Chem. Front.*, 2023, **7**, 1599-1606.
5. H.Y. Zhang and R.G. Xiong, Three-dimensional narrow-bandgap perovskite semiconductor ferroelectric methylphosphonium tin triiodide for potential photovoltaic application, *Chem. Commun.*, 2023, **59**, 920-923.
6. P.F. Li, Y.Y. Tang, W.Q. Liao, H.Y. Ye, Y. Zhang, D.W. Fu, Y.M. You and R.G. Xiong, A semiconducting molecular ferroelectric with a bandgap much lower than that of $BiFeO_3$, *NPG Asia Mater.*, 2017, **9**, e342.
7. S. G. Han, J. Zhang, Z. H. Sun, C. M. Ji, W. C. Zhang, Y. Y. Wang, K. W. Tao, B. Teng and J. H. Luo, Lead-Free Hybrid Material with an Exceptional Dielectric Phase Transition Induced by a Chair-to-Boat Conformation Change of the Organic Cation, *Inorg. Chem.*, 2017, **56**, 13078-13085.
8. L.L. Chu, T. Zhang, Y.F. Gao, W. Y. Zhang, P. P. Shi, Q. Ye and D. W. Fu, Fluorine Substitution in Ethylamine Triggers Second Harmonic Generation in Noncentrosymmetric Crystalline $[NH_3CH_2CH_2F]_3BiCl_6$, *Chem. Mater.*, 2020, **32**, 6968-6974.
9. R. Jakubas, A. Gagor, M. J. Winiarski, M. Ptak, A. Piecha-Bisiorek and A. Cizman, Ferroelectricity in Ethylammonium Bismuth-Based Organic-Inorganic Hybrid: $(C_2H_5NH_3)_2[BiBr_5]$, *Inorg. Chem.*, 2020, **59**, 3417-3427.
10. Y. Rakita, O. Bar-E and E. Meirzadeh and D. Cahen, Tetragonal $CH_3NH_3PbI_3$ is ferroelectric, *Proc. Natl. Acad. Sci. USA*, 2017, **114**, 5504-12.
11. T.T. Sha, Y.A. Xiong, Q. Pan, X.J. Song, J. Yao, S.R. Miao, Z.Y. Jing, Z.J. Feng, Y.M. You and R.G. Xiong, Fluorinated 2D lead iodide perovskite ferroelectrics, *Adv. Mater.*, 2019, **31**, 1901843.
12. Y.L. Zeng, X.Q. Huang, C.R. Huang, H. Zhnag, F. Wang and Z.X. Wang, Unprecedented 2D homochiral hybrid lead-iodide perovskite thermochromic ferroelectrics with ferroelastic switching, *Angew. Chem. Int. Ed.*, 2021, **60**, 10730-5.
13. J.Y. Liu, M.M. Lun, Z.J. Wang, J.Y. Li, K. Ding, D.W. Fu, H.F. Lu and Y. Zhang, The H/F substitution strategy can achieve large spontaneous polarization in 1D hybrid perovskite ferroelectrics, *Chem. Sci.*, 2024, **15**, 16612.
14. H. Zhang, Q.L. Li, Y.H. Tan, Y. Z. Tang, X.W. Fan, J.J. Luo, F.X. Wang and M.Y. Wan, High-temperature ferroelasticity and photoluminescence in a 2D monolayer perovskite compound: $(C_5NH_8Br)_2PbBr_4$, *Inorg. Chem.*, 2023, **62**, 10847-10853.
15. M.J. Yang, H. Cheng, Y.Q. Xu, M.Z. Li and Y. Ai, A hybrid organic-inorganic perovskite with robust SHG switching, *Chin. Chem. Lett.*, 2022, **33**, 2143-2146.

16. S.S. Wang, L.N. Li, W. Weng, C.M. Ji, X.T. Liu, Z.H. Sun, W.X. Lin, M.C. Hong and J.H. Luo, Trilayered Lead Chloride Perovskite Ferroelectric Affording Self-Powered Visible-Blind Ultraviolet Photodetection with Large Zero-Bias Photocurrent, *J. Am. Chem. Soc.*, 2020, **142**, 55-59.
17. X.N. Hua, W.Q. Liao, Y.Y. Tang, P.F. Li, P.P. Shi, D.W. Zhao and R.G. Xiong, A Room-Temperature Hybrid Lead Iodide Perovskite Ferroelectric, *J. Am. Chem. Soc.*, 2018, **140**, 12296-12302.
18. R. Chakraborty, P. K. Rajput, G. M. Anilkumar, S. Maqbool, R. Das, A. Rahman, P. Mandal and A. Nag, Rational Design of Non-Centrosymmetric Hybrid Halide Perovskites, *J. Am. Chem. Soc.*, 2023, **145**, 1378-1388.
19. H.Y. Zhang, X.J. Song, X.G. Chen, Z.X. Zhang, Y.M. You, Y.Y. Tang and R.G. Xiong, Observation of Vortex Domains in a Two-Dimensional Lead Iodide Perovskite Ferroelectric, *J. Am. Chem. Soc.*, 2020, **142**, 4925-4931.
20. F.L. Zhou, S. T. Song, M.M. Lun, H. N. Zhu, K. Ding, S.N. Cheng, D.W. Fu and Y. Zhang, A hybrid multifunctional perovskite with dielectric phase transition and broadband red-light emission, *J. Mol. Struct.*, 2021, **1239**, 130468.
21. M.Y. Wan, Y.Z. Tang, Y.H. Tan, F.X. Wang, Y.N. Li, L.J. Wang, J. Liao and M.N. Wang, Excellent Switchable Properties, Broad-Band Emission, Ferroelectricity, and High $T_c$ in a Two-Dimensional Hybrid Perovskite: $(4,4\text{-DCA})_2PbBr_4$ Exploited by H/F Substitution, *Inorg. Chem.*, 2023, **62**, 12525-12533.
22. H.Y. Zhang, X.J. Song, X.G. Chen, Z, X, Zhang, Y. M. You, Y. Y. Tang and R. G. Xiong, Observation of Vortex Domains in a Two-Dimensional Lead Iodide Perovskite Ferroelectric, *J. Am. Chem. Soc.*, 2020, **142**, 4925-4931.
23. P.P. Shi, S.Q. Lu, X.J. Song, X.G. Chen, W.Q. Liao, P.F. Li, Y.Y. Tang and R.G. Xiong. Two-dimensional organic-inorganic perovskite ferroelectric semiconductors with fluorinated aromatic spacers. *J. Am. Chem. Soc.*, 2019, **141**, 18334-40.